

Unseen from Seen: Rewriting Observation-Instruction Using Foundation Models for Augmenting Vision-Language Navigation

Ziming Wei*, Bingqian Lin*, Yunshuang Nie, Jiaqi Chen, Shikui Ma, Hang Xu, Xiaodan Liang†

Abstract—Data scarcity is a long-standing challenge in the Vision-Language Navigation (VLN) field, which extremely hinders the generalization of agents to unseen environments. Previous works primarily rely on additional simulator data or web-collected images/videos to improve the generalization. However, the simulator environments still face limited diversity, and the web-collected data often requires extensive labor to remove the noise. In this paper, we propose a Rewriting-driven Augmentation (RAM) paradigm for VLN, which directly creates the unseen observation-instruction pairs via rewriting human-annotated training data. Benefiting from our rewriting mechanism, new observation-instruction can be obtained in both simulator-free and labor-saving manners to promote generalization. Specifically, we first introduce Object-Enriched Observation Rewriting, where we combine Vision-Language Models (VLMs) and Large Language Models (LLMs) to derive rewritten object-enriched scene descriptions, enabling observation synthesis with diverse objects and spatial layouts via Text-to-Image Generation Models (T2IMs). Then, we propose Observation-Contrast Instruction Rewriting, which generates observation-aligned rewritten instructions by requiring LLMs to reason the difference between original and new observations. We further develop a mixing-then-focusing training strategy with a random observation cropping scheme, effectively enhancing data distribution diversity while suppressing augmentation data noise during training. Experiments on both the discrete environments (R2R, REVERIE, and R4R datasets) and continuous environments (R2R-CE dataset) show the superior performance and impressive generalization ability of our method. Code is available at <https://github.com/SaDiI13/VLN-RAM>.

Index Terms—Vision-Language Navigation, Data Augmentation, Foundation Models, Text-to-Image Generation.

I. INTRODUCTION

Vision-Language Navigation (VLN) [1], [2], [3], [4], as a critical research path to achieve embodied intelligence, defines the task that requires an embodied agent to navigate through complex 3D environments following natural language instructions. To enable VLN agents to learn

the observation-instruction alignment knowledge and navigation skills, researchers have provided elaborately annotated trajectory-instruction data from the simulator environments [5] for navigation training. Nevertheless, the limited amount of high-quality manually annotated VLN data, i.e., the data scarcity issue, greatly harms the generalization of existing agents to unseen environments with various possible spatial layouts and cooccurrence objects.

To address the data scarcity problem, prior studies have investigated numerous data augmentation strategies, which can be roughly divided into two categories: simulator-based and web-based. Simulator-based methods [6], [7], [8], [9], [10], [11] rely on the original Matterport3D [5] environment or additional simulators like HM3D [12] and Gibson [13] to perform augmentation trajectory sampling and use the Speaker [7] model for instruction generation. In contrast, web-based approaches [14], [15] collect room images or room-tour videos from the web for trajectory augmentation, and adopt the template-based strategy to generate instructions. Despite the promising performance improvement, these approaches still have the following limitations. For trajectory generation, the simulator data is always constrained in specific environments and hard to extend to various scenarios. On the other hand, web images/videos usually contain extensive noise and demand labor-intensive data cleaning. For instruction augmentation, Speaker-generated instructions are usually uninformative while template-based instructions may have limited flexibility.

In this paper, we propose a new data augmentation framework, dubbed **Rewriting-driven Augmentation (RAM)**, which generates the unseen observation-instruction pairs via rewriting original human-annotated data. Our RAM enables observation-instruction rewriting in both *simulator-free* and *labor-saving* manners, powered by an elegant combination for various foundation models. As shown in Fig. 1, our RAM encompasses two core modules. Firstly, we introduce **Object-Enriched Observation Rewriting**, which synthesizes new observations with different spatial layouts and objects out of the simulator while requiring no labor-intensive postprocessing procedures. To achieve this, we combine Vision-Language Models (VLMs) and Large Language Models (LLMs) to obtain object-enriched rewritten observation descriptions. Then we feed them to Text-to-Image Generation Models (T2IMs) to perform new observation generation. Secondly, we conduct **Observation-Contrast Instruction Rewriting**, where we ask LLMs to generate observation-aligned instructions by reasoning the difference between original and new observation

*These two authors contribute equally to this work.

†Xiaodan Liang is the corresponding author.

Ziming Wei, Yunshuang Nie and Xiaodan Liang are with Shenzhen Campus of Sun Yat-sen University, Shenzhen, China. (e-mail: weizm3@mail2.sysu.edu.cn; nieysh@mail2.sysu.edu.cn; liangxd9@mail.sysu.edu.cn).

Bingqian Lin is with the Shanghai Jiao Tong University. (e-mail: linbq666@sjtu.edu.cn).

Jiaqi Chen is with the University of Hong Kong. (e-mail: jqchen@cs.hku.hk).

Shikui Ma is with Dataa Robotics company. (e-mail: maskey.bj@gmail.com).

Hang Xu is with Huawei Noah's Ark Lab. (e-mail: chromexbjxh@gmail.com).

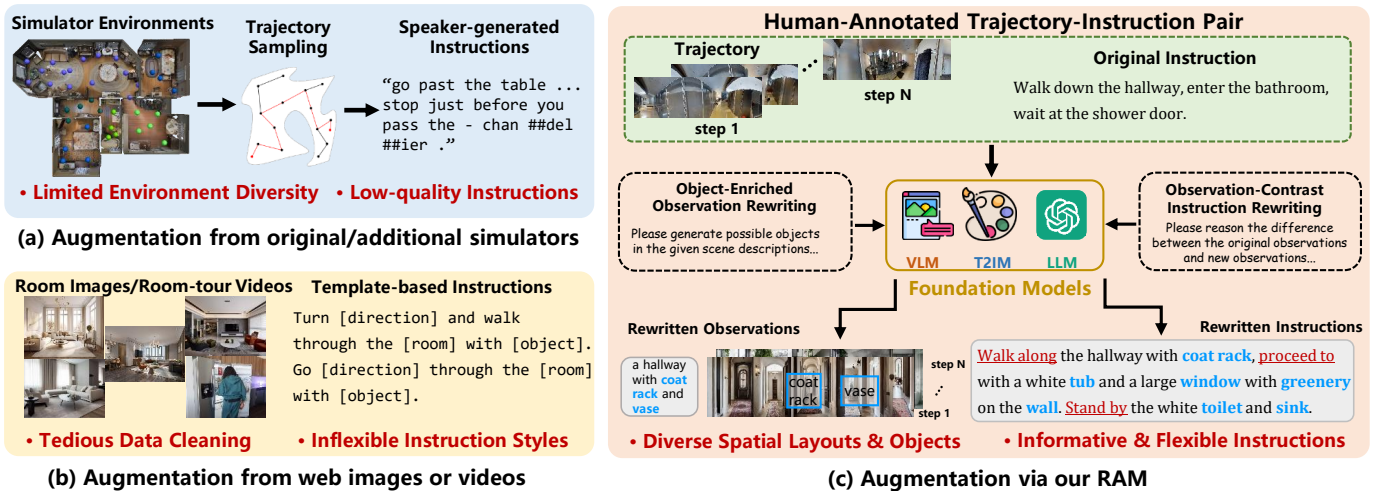


Fig. 1. Comparison of our RAM with typical VLN data augmentation approaches: (a) Augmentation from original/additional simulators and (b) Augmentation from web images or videos. Rather than these methods that may be limited in specific simulator environments or struggle with tedious data cleaning, our RAM (c) empowers simulator-free and labor-saving data augmentation by rewriting human-annotated data to generate unseen observation-instruction pairs. The generated scene objects and the newly introduced objects mentioned in the rewritten instructions are denoted by blue boxes/fonts. New actional representations in the rewritten instructions are denoted by red underlined fonts. The mixing-then-focusing training strategy is omitted in this figure.

descriptions obtained via VLMs. We also require the LLMs to change the representations of actional descriptions and syntax architecture for generating new instructions. Therefore, our rewritten instructions are more informative with flexible representations. To strengthen the diversity of data distribution while suppressing the negative impact of rewritten data (e.g., the inherent generation noise brought by T2IMs) for improving training, we further develop a **mixing-then-focusing training scheme** accompanied by a random observation cropping strategy. As a result, our rewritten data can bring significant performance gains with only a small scale.

Experimental results on R2R [1], REVERIE [2], and R4R [16] show the superior performance of RAM over existing methods especially in unseen scenarios, demonstrating the effectiveness of our proposed rewriting-driven augmentation paradigm in improving generalization. Through only small-scale data augmentation, our RAM achieves comparable or even better performance to a recent state-of-the-art method [10] that relies on large-scale data from additional simulators on R2R and REVERIE. The transfer of our RAM to the R2R-CE [17] dataset further reveals the promising generalization ability of the proposed method.

To summarize, the main contributions of this work are:

- We propose RAM, a novel VLN data augmentation paradigm that rewrites the human-annotated data to generate unseen observation-instruction pairs. The proposed framework integrates a series of foundation models to perform rewriting without any reliance on the simulator environments or web-collected data.
- We provide a detailed evaluation of different data fusion schemes for training. We also introduce a two-stage mixed training strategy with a random observation cropping scheme, which sufficiently activates the advantage of our rewritten data while simultaneously mitigating its inherent noise to boost training.
- RAM shows impressive generalization ability on multiple

VLN datasets. It achieves comparable or even better performance to a recent SOTA data augmentation method by introducing ~ 100 times less augmentation data.

The remainder of this paper is organized as follows. Section II provides a brief review of the related work. Section III describes the problem setup of the VLN task and then introduces our proposed method. Section IV presents the experimental setup and results. Section V concludes the paper and gives some outlook for future work.

II. RELATED WORK

A. Vision-Language Navigation

Vision-Language Navigation (VLN) is a challenging task that asks an agent to follow human instructions to navigate to the target position. As a core task in the Embodied AI area, VLN has drawn increasing research interest in recent years. Early methods use a sequence-to-sequence architecture [1] to build VLN models with cross-modal alignment modules [18], [19] and effective training mechanisms [20], [21], [22], [23] such as reinforcement learning [6], [20], contrastive learning [24], [25], [26], adversarial learning [11], [27], etc. For example, RCM [20] introduces a reinforced cross-modal matching approach to enforce the cross-modal grounding both locally and globally via reinforcement learning. AuxRN [21] proposes multiple self-supervised auxiliary learning tasks to explore the rich information in the VLN environment. DISH [28] introduces a hierarchical reinforcement learning method for VLN, decomposing tasks into subgoals via a manager-worker framework to alleviate the reward sparsity. GL-VLN [29] proposes a global normalization strategy with two score functions to rerank beam-search trajectories in VLN, addressing trajectory-level score bias. VPG [30] proposes a meta-learning-based visual perception generalization strategy with MAML and feature-wise affine transformation, achieving effective skill transfer in VLN tasks.

Inspired by the great success of vision-language pre-training [31], [32], [33], [34], [35], recent approaches use transformer-based architecture and devise domain-specific proxy tasks to boost the performance of VLN models [36], [37], [38], [39], [40], [41], [42], [43]. PREVALENT [37] constructs large-scale image-text-action triplets to pretrain the agent. VLN \odot BERT [36] enables the agent to recognize time-dependent input by introducing a recurrent function. HAMT [38] constructs a history-aware multimodal transformer for long-horizon navigation history encoding. However, most existing methods rely on domain-specific VLN data obtained from limited simulator environments, and therefore cannot generalize well to various unseen scenarios.

Some recent works have attempted to unleash the rich world knowledge from the foundation models, such as Large Language Models (LLMs) [44], [45] and Vision Language Models (VLMs) [46], [47], to improve the generalization ability of the VLN agent [48], [49], [50], [51]. For example, NavGPT [48] builds a purely GPT4-based navigation agent that reasons the action decision based on the textual represented visual observations and navigational histories. DiscussNav [49] incorporates multiple foundation models like InstructBLIP [47] and GPT4 [45] to address different navigation inputs and produce comprehensive reasoning for decision.

In this paper, we propose a rewriting-based VLN data augmentation approach driven by foundation models to mitigate the data scarcity issue of VLN and improve the generalization ability of navigation agents. Rather than using foundation models for navigation decisions directly which need frequent queries, we adopt the foundation models for VLN data augmentation and therefore leading to a low-frequency query and reducing the cost significantly. Moreover, in contrast to existing zero-shot LLM-based VLN approaches [48], [49], [50], our approach effectively avoids the domain gap between foundation models and the VLN task through training supervised-learning-based navigation agents [39], [38] on both the human-annotated training data and our augmentation data.

B. Data Augmentation in VLN

Due to the collection difficulty of large-scale human-annotated trajectory-instruction pairs, data scarcity stands as a crucial challenge in VLN and researchers have adopted various augmentation strategies to tackle this issue. In this work, we mainly divide these approaches into two branches. The first branch is simulator-based [6], [7], [8], [9], [10], [52], i.e., the augmentation data comes from the original Matterport3D [5] simulator or external simulators like HM3D [12]. For example, Speaker-Follower [7] samples augmentation trajectories randomly in Matterport3D environment and trains a Speaker model to collect paired instructions. ScaleVLN [10] synthesizes 4.9 million trajectory-instruction pairs from HM3D [12] and Gibson [13] simulators. However, the sampled trajectories are still constrained by specific simulator environments. Another branch is web-based, which collects large-scale images or videos from the web. AirBert [15] introduces room images from Airbnb and Youtube-VLN [14] collects room-tour videos on YouTube for enhancing environmental diversity,

respectively. Nevertheless, the noise of these web resources harms training and brings a heavy burden for data cleaning.

In contrast to the above mentioned approaches, in this work, we propose to generate unseen observation-instruction pairs via rewriting human-annotated training data, fulfilling simulator-free and labor-saving data augmentation for the VLN task. A recent work [53] also synthesizes new observations out of the simulator by introducing T2IMs, accompanied by Speaker-based instruction generation. However, our work is different from it in two aspects: 1) Our framework is rewriting-driven, where we rewrite observation descriptions and instructions to enable object-enriched observation generation and training-free instruction augmentation. 2) Our introduced mixing-then-focusing training strategy with the random observation cropping scheme effectively enhances the data distribution diversity while simultaneously restraining the negative impact of the augmentation data.

C. LLM-Driven Robotic Data Generation

Thanks to the rich commonsense knowledge and powerful reasoning ability, LLMs have been proven a helpful data generation tool for alleviating the data shortage in robotic tasks by some recent works [54], [55], [56], [57], [58]. DIAL [54] employs GPT-3 to perform instruction augmentation by producing rephrased instructions guided by world knowledge. GenSim [55] uses GPT-4 to generate a task curriculum to enrich the existing benchmark by ten times. Holodeck [56] leverages GPT-4 to generate spatial relational constraints between objects to create diverse scenes. RoboGen [57] utilizes GPT-4 to produce task proposals and scene configurations for realizing generative simulation. EnvGen [58] creates new training environments by prompting GPT-4 to generate a set of environment configurations which can be parsed by the simulator.

In this work, we harness the physical world knowledge, reasoning ability, and language skills of the LLM, and integrate the LLM with other foundation models like T2IMs for conducting observation-instruction rewriting for VLN. As a result, our rewritten observations will have reasonable and diverse objects conforming to real-world scenarios. Moreover, the rewritten instructions will be more flexible and informative compared to Speaker-generated instructions and template-based instructions in previous VLN approaches.

III. METHOD

In this section, we first describe the VLN problem setup (Section III-A) and then delve into the details of our RAM. The overview of RAM is illustrated in Fig. 2. Specifically, given a human-annotated trajectory-instruction pair, RAM first performs Object-Enriched Observation Rewriting (Section III-B), where Vision-Language Models (VLMs) and Large Language Models (LLMs) are introduced to generate object-enriched rewritten observation descriptions, based on which new observations are synthesized through an efficient panorama-to-view strategy via Text-to-Image Generation Models (T2IMs). Then, RAM conducts Observation-Contrast Instruction Rewriting (Section III-C), which collects grounded

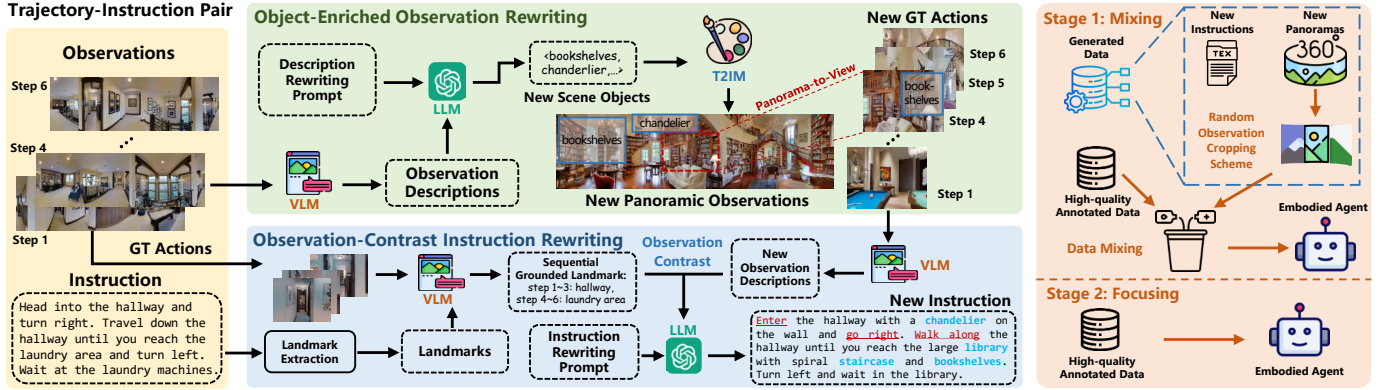


Fig. 2. Overview of our **R**ewriting-driven **A**ugmentation (**RAM**) paradigm. For Object-Enriched Observation Rewriting, we collect object-enriched rewritten scene descriptions based on VLMs and LLMs. Then we feed the rewritten descriptions to T2IMs for synthesizing new observations via an efficient panorama-to-view scheme. During Observation-Contrast Instruction Rewriting, we ask the LLMs to perform observation contrast by reasoning the difference between original and new observation descriptions to generate new instructions. We further introduce a mixing-then-focusing strategy with a random observation cropping scheme for combining our rewritten trajectory-instruction pairs with human-annotated data for training. Newly generated objects and actional representations in the rewritten instruction are denoted in **blue** and **red underlined** fonts, respectively.

landmark information and observation descriptions respectively for the original and new trajectories, and asks the LLMs to contrast the difference between them to produce rewritten instructions. After collecting rewritten observation-instruction pairs, a two-stage mixing-then-focusing training strategy with a random observation cropping scheme is developed to effectively combine the rewritten data with the original data for training (Section III-D). A notation summarization of variables appeared in this section is provided in Table I.

TABLE I
NOTATION SUMMARIZATION OF VARIABLES.

Variables	Notations
instruction	I
observation	O_t
scene description	C_t
rewritten object-enriched scene description	C_t^r
rewritten observation	O_t^r
ground-truth action (observation)	G_t
grounded landmark for the ground-truth action (observation)	U_t
scene description of the rewritten observation	C_t^r
rewritten instruction	I^r
scene description rewriting prompt	P^c
instruction rewriting prompt	P^i

A. VLN Problem Setup

In the discrete VLN task, an agent needs to explore the navigation connection graph $\mathcal{G} = (V, E)$, moving from a starting node to a target node following a given language instruction. V and E represent the nodes and edges in the navigation connectivity graph. At timestep t , the agent receives a panoramic observation O_t containing K single-view observations $O_{t,k}$, i.e., $O_t = \{O_{t,k}\}_{k=1}^K$. There are N navigable views among K views. The action space consists of the navigable views and a ‘STOP’ action, and the agent chooses one as the action prediction a_t from the action space at different timestep t .

The continuous VLN is established on the Habitat [12] simulator, where the agent can navigate to any points rather than the predefined graph nodes in the environment. Following existing works [38], [10], we adopt a pretrained waypoint predictor [59] to generate navigable waypoints in continuous environments, similar to that in the discrete VLN setting.

During VLN training, the agent is fed with trajectory-instruction pairs to learn cross-modal alignment knowledge and navigational skills, optimized by imitation learning algorithms or reinforcement learning algorithms [36], [38], [39].

B. Object-Enriched Observation Rewriting

Many previous works [52], [8], [53] focus on how to generate or introduce more environments for VLN training. For example, EnvEdit [52] and REM [8] edit the existing environments by changing room style and object appearances or mixing up environments. However, these approaches do not change spatial layouts among different objects or introduce objects with new categories essentially. In our RAM, we propose Object-Enriched Observation Rewriting, which can extend the original scene to new scenes with diverse objects and spatial layouts efficiently for improving generalization.

Object-Enriched Observation Rewriting consists of two primary procedures, namely Object-Enriched Scene Description Rewriting and Panorama-to-View Observation Generation. During Object-Enriched Scene Description Rewriting, we utilize VLMs to collect scene description C_t for original observation O_t , then we leverage LLMs to provide object cooccurrence knowledge and generate rewritten object-enriched scene descriptions C_t^r . In Panorama-to-View Observation Generation, we obtain rewritten observations O_t^r by feeding C_t^r to T2IMs to directly synthesize rewritten panoramas, followed by a simple panorama discretization algorithm to produce new single-view observations.

Object-Enriched Scene Description Rewriting. For a human-annotated trajectory-instruction pair, we first use the Vision-Language Model (VLM) to collect panoramic observation descriptions during different navigation timesteps in the

trajectory. For panoramic observation O_t at timestep t , we get the scene description C_t of O_t by:

$$C_t = \text{VLM}(O_t). \quad (1)$$

Then we construct the scene description rewriting prompt P^c , which contains the task definition formed as “Generate rewritten descriptions by adding the possible objects that may exist in the scene for the given scene description”.

To constrain the LLM to explicitly indicate possible scene objects in its generated scene descriptions, we ask the LLM in P^c to generate both newly added objects $\{B_{t,n}\}_{n=1}^N$ and rewritten scene descriptions C_t^r by feeding an in-context task example, as shown in Fig. 3. Additionally, to encourage the subsequent generated observations via T2IMs based on the rewritten scene descriptions C_t^r to indicate different salient objects, which can enhance the diversity potentially, we also require the LLM in P^c to change the representation of original scene descriptions for highlighting different objects. The reason why we ask the LLM to explicitly specify objects added to the synthetic scene is to facilitate adding objects with specific numbers as well as manually checking the generation quality of rewritten scene descriptions. And we do not utilize the outputs of added objects in the subsequent stages of our method. Therefore, with our scene description rewriting prompt P^c and the original scene description C_t , we obtain the rewritten object-enriched scene descriptions C_t^r accompanied by added objects $\{B_{t,n}\}_{n=1}^N$ by:

$$C_t^r, \{B_{t,n}\}_{n=1}^N = \text{LLM}(C_t, P^c), \quad (2)$$

where N is the number of added objects.

Panorama-to-View Observation Generation. We develop a panorama-to-view generation strategy for obtaining rewritten observations O_t^r , i.e., we first feed the rewritten object-enriched scene description C_t^r to a panoramic T2IM once to collect rewritten panoramas, then we perform the panorama discretization to extract K single-view observations, i.e., $O_t^r = \{O_{t,k}^r\}_{k=1}^K$. A recent work [53] adopts a view-to-panorama generation manner, which needs to query the T2IM multiple times to generate each single-view observation, as well as stitch them into a panorama to improve view consistency. In contrast, our directly generated panoramas can naturally own view consistency.

For panorama generation, we choose MultiDiffusion [60], which is capable of generating images with desired aspect ratios and informative contents to generate the panoramic images. We employ the Equirec2Perspec algorithm¹ to discretize a panoramic image into 36 perspective images following the same setting in VLN [1]. Initially, the Equirec2Perspec algorithm utilizes the camera parameters, encompassing the Field of View (FOV), heading (θ), and elevation (ϕ), to calculate the inverse matrix of the camera’s projection matrix, denoted as J_{inv} , and the rotation matrix, denoted as R :

$$\begin{aligned} J_{inv} &= \text{MC}_{\text{proj}}(\text{FOV}, \theta, \phi), \\ R &= \text{MC}_{\text{rot}}(\theta, \phi), \end{aligned} \quad (3)$$

where $\text{MC}_{\text{proj}}(\cdot)$ is the camera’s projection matrix calcula-

¹<https://github.com/fuenwang/Equirec2Perspec>

Object-Enriched Scene Description Rewriting

Task: Generate rewritten descriptions by adding the possible objects that may exist in the scene for the given scene description and changing the original representation.

Scene description: a bathroom that has mirrors on the walls

Added objects: vanity, sink, faucet

Rewritten descriptions: A spacious bathroom featuring a large vanity with a marble countertop and double sinks, reflecting off the expansive mirrors on the walls, complemented by chrome faucets and a tiled backsplash.

Scene description: C_t

Added objects:

Rewritten descriptions:

Observation-Contrast Instruction Rewriting

Task: Rewrite the original instruction by replacing the object(scene) in the original instruction with the one in the new observation according to the matched step information. You should also modify the actional representations to their synonyms.

Landmarks in original trajectory:

Step1: workshop; Step2: workshop;

Step3: black leather chair; Step4: black leather chair.

New observation descriptions:

Step1: a modern kitchen with stainless steel appliances and a large island.

Step2: the foyer of a large house with high ceilings, windows, doors and a fireplace.

Step3: the interior of a modern house with large windows, a living room and kitchen.

Step4: a dining table and chairs in a modern kitchen and dining area of an apartment.

Original instruction:

Leave the workshop and head to the black leather chair. Stop next the chair and the red wicker chairs.

Rewritten instruction:

Go out of the kitchen and walk forward to the large windows. Stand by a dining table with chairs.

Landmarks in original trajectory: $\{U_t\}_{t=1}^T$

New observation descriptions: $\{C_t^r\}_{t=1}^T$

Original instruction: I

Rewritten instruction:

Fig. 3. Prompts for Object-Enriched Scene Description Rewriting and Observation-Contrast Instruction Rewriting.

tion function and $\text{MC}_{\text{rot}}(\cdot)$ is the rotation matrix calculation function.

Then the algorithm takes J_{inv} , R , and multiple processing functions to convert pixel coordinates on the panoramic image O_t^r to 3D point coordinates on the spherical surface, and then transform it to two-dimensional coordinates on the image plane to generate the single-view images $\{O_{t,k}^r\}_{k=1}^K$:

$$\{O_{t,k}^r\}_{k=1}^K = \text{Equirec2Perspec}(J_{inv}, R, O_t^r), \quad (4)$$

where the Equirec2Perspec function is the synthesis of a series of coordinate conversion functions. As shown in Fig. 2, the generated single-view images (see “New GT Actions”) have a similar field of view effect to the original single-view images in the Matterport3D [5] simulator.

C. Observation-Contrast Instruction Rewriting

As our newly generated panoramic observations of the trajectory are different from the original observations, the original paired instruction will not be aligned well with our new panoramic observations. In contrast to previous Speaker-based [52], [53], [7] or template-based [15], [14] instruction augmentation approaches, in this work, we introduce Observation-Contrast Instruction Rewriting to generate rewritten instructions I^r based on the rewritten observations $\{O_t^r\}_{t=1}^T$, where T is the navigation step number for a specific trajectory.

Specifically, we first perform Sequential Landmark Grounding, i.e., obtaining the grounded landmark U_t for each observation O_t in the original trajectory from the original instruction

I. Then, we conduct New Observation Description Collection to derive descriptions C'_t for the rewritten observations O'_t . Finally, we obtain rewritten instructions I^r by asking the LLM to: 1) contrast each U_t and C'_t to replace U_t in I with the landmark appearing in C'_t at the appropriate timestep, and 2) change the original actional representations in I to their synonyms. Consequently, our rewritten instructions can be observation-aligned with flexible representations. Moreover, benefiting from rewriting human-annotated instructions, the generated instructions can be essentially more informative.

Sequential Landmark Grounding. Since the landmarks mentioned in the instruction exist in the ground-truth action (observation) generally, for each ground-truth observation, we find its matched landmark in the instruction to perform sequential landmark grounding. Concretely, we first use an LLM to extract the sequential landmarks $U = \{U_k\}_{k=1}^M$ from the original instruction I like that in [61], where M is the size of the landmark list. Denote the ground-truth action (observation) at timestep t extracted from the original observation O_t as G_t . For each G_t , we employ a VLM [46] to find its matched landmark U_t by taking the landmark U_k which has maximum similarity with G_t :

$$U_t = \operatorname{argmax}_{U_k} \operatorname{Sim}(F^v(G_t), F^t(U_k)), \quad (5)$$

where F^t and F^v are the text encoder and the image encoder of the VLM, respectively. We represent the sequential grounded landmark information as $\{U_t\}_{t=1}^T$, where T is the navigation step number for a specific trajectory.

New Observation Description Collection. After sequential landmark grounding for each ground-truth action (observation) G_t in the original trajectory to collect $\{U_t\}_{t=1}^T$, we extract the ground-truth action (observation) G'_t which has the same position as G_t from the rewritten observations O'_t . Then, we adopt the VLM used during Object-Enriched Scene Description Writing to generate the description C'_t for the ground-truth action (observation) G'_t like Eq. 1. We represent the sequential observation descriptions for new ground-truth observation sequence $\{G'_t\}_{t=1}^T$ as $\{C'_t\}_{t=1}^T$.

Instruction Rewriting by Observation Contrast. As shown in Fig. 3, we build the instruction rewriting prompt P^i with the task description of “Rewrite the original instruction by replacing the object (scene) in the original instruction with the one in the new observation...”, followed by an in-context task example, which teaches the LLM to perform observation contrast as well as change the representations of actional descriptions to produce rewritten instructions. Therefore, with our instruction rewriting prompt P^i , the grounded landmark information $\{U_t\}_{t=1}^T$, the new observation descriptions $\{C'_t\}_{t=1}^T$, and the original instruction I , the rewritten instruction I^r is acquired by:

$$I^r = \operatorname{LLM}(\{U_t\}_{t=1}^T, \{C'_t\}_{t=1}^T, I, P^i) \quad (6)$$

D. Mixing-then-Focusing Training Mechanism

After obtaining the rewritten data, one simple way is to mix it with the original data for training directly. However, due to the inherent deficiency of foundation models, e.g., the repeated object generation issue of the panoramic T2IMs [62],

arbitrarily introducing rewritten data may bring unexpected noise. Therefore, we introduce an effective two-stage mixing-then-focusing training mechanism, where we mix the original data with rewritten data in Stage 1, and use pure original data to reduce the noise impact in Stage 2. During stage 1, we additionally introduce a random observation cropping scheme to serve as a data augmentation method, i.e., for a rewritten panorama, we randomly crop it into large patches, and combine the patches from different panoramas to form new panoramas. This further strengthens the diversity of rewritten data while mitigating the repeated object generation issue of the T2IMs. Denote the original training data as $\{\{O_t\}_{t=1}^T, I\}$ and our rewritten data as $\{\{O'_t\}_{t=1}^T, I^r\}$, where T is the step number of a trajectory. The navigation losses for the two stages \mathcal{L}_{s1} and \mathcal{L}_{s2} are calculated respectively by:

$$\mathcal{L}_{s1} = E^n \left(\left\{ \{O_t\}_{t=1}^T, I \right\}, \left\{ \operatorname{RC}(\{O'_t\}_{t=1}^T), I^r \right\} \right), \quad (7)$$

$$\mathcal{L}_{s2} = E^n \left(\left\{ \{O_t\}_{t=1}^T, I \right\} \right), \quad (8)$$

where E^n represents the navigation agent and $\operatorname{RC}(\cdot)$ denotes our random observation cropping scheme.

IV. EXPERIMENTS

A. Experimental Setup

1) *Datasets:* We mainly evaluate our RAM on three discrete VLN benchmarks: R2R [1], REVERIE [2], and R4R [16]. R2R contains 90 indoor scenes with 7189 trajectories. Each trajectory is accompanied by 3 step-by-step instructions. On average, an instruction contains 32 words, and each ground-truth path is formed by seven nodes with a total length of $10m$. REVERIE replaces the fine-grained instructions in R2R with high-level instructions that are only related to the target position and object. R4R creates longer instructions and trajectories by concatenating two adjacent tail-to-head trajectories in R2R. Both R2R and REVERIE split the evaluation set into Val Seen, Val Unseen, and Test Unseen, while R4R only split the evaluation set into Val Seen and Val Unseen. “Val Seen” means new trajectory-instruction pair data but collected from the same houses as those in the training dataset. On the other hand, “Val Unseen” and “Test Unseen” stand for the entirely different VLN data collected from additional houses which are different from the houses in the training dataset.

We also extend our RAM to R2R-CE [17], which transfers the discrete trajectories in R2R to continuous 3D scans rendered by Habitat [63] simulator. The R2R-CE dataset contains 16k instruction-trajectory pairs after removing non-transferable paths.

2) *Evaluation Metrics:* We use the following metrics for evaluation on R2R and R2R-CE: 1) Trajectory Length (TL): the average length of the agent’s navigated path in meters, 2) Navigation Error (NE): the average distance in meters between the agent’s destination and the target viewpoint, 3) Success Rate (SR): the ratio of success, where the agent stops within three meters of the target point, and 4) Success rate weighted by Path Length (SPL): success rate normalized by the ratio between the length of the shortest path and the predicted

TABLE II

COMPARISON WITH EXISTING METHODS ON R2R. *: 900 EXTRA SIMULATOR SCENES FOR TRAINING AND USING CLIP ViT H/14 AS IMAGE FEATURES. †: USING CLIP ViT B/16 AS IMAGE FEATURES. ‡: USING CLIP ViT L/14 AS IMAGE FEATURES.

Method	Val Seen				Val Unseen				Test Unseen			
	TL	NE ↓	SR ↑	SPL ↑	TL	NE ↓	SR ↑	SPL ↑	TL	NE ↓	SR ↑	SPL ↑
ScaleVLN* [10]	13.24	2.12	81	75	14.09	2.09	81	70	13.93	2.27	80	70
Seq2Seq [1]	11.33	6.01	39	-	8.39	7.81	22	-	8.13	7.85	20	18
Speaker-Follower [7]	-	3.36	66	-	-	6.62	35	-	14.82	6.62	35	28
EnvDropout [6]	11.00	3.99	62	59	10.70	5.22	52	48	11.66	5.23	51	47
HOP [64]	11.51	2.46	76	70	12.52	3.79	64	57	13.29	3.87	64	58
Airbert [15]	11.09	2.68	75	70	11.78	4.01	62	56	12.41	4.13	62	57
HAMT [38]	11.15	2.51	76	72	11.46	3.62	66	61	12.27	3.93	65	60
EnvEdit [52]	11.18	2.32	77	74	11.13	3.24	69	64	11.90	3.59	68	64
TD-STP [41]	-	2.34	77	73	-	3.22	70	63	-	3.73	67	61
DUET [39]	12.32	2.28	79	73	13.94	3.31	72	60	14.73	3.65	69	59
YouTube-VLN [14]	-	-	-	-	14.58	2.90	74	62	16.13	3.44	72	60
PanoGen [53]	-	-	-	-	13.40	3.03	74	64	14.38	3.31	72	62
DUET† [39] (baseline)	13.86	2.12	80.80	73.64	16.22	3.06	72.37	58.75	-	-	-	-
RAM†(ours)	11.50	1.95	82.17	77.70	13.33	2.96	73.65	63.13	14.69	3.34	71	61
DUET‡ [39] (baseline)	11.64	1.92	82.76	78.17	13.05	3.07	73.22	64.49	-	-	-	-
RAM‡(ours)	11.97	1.85	82.47	77.98	13.39	2.66	76.29	66.39	14.50	3.08	75	65

TABLE III

NAVIGATION AND OBJECT GROUNDING PERFORMANCE ON REVERIE. *: 900 EXTRA SIMULATOR SCENES FOR TRAINING. ‡: USING CLIP ViT L/14 AS IMAGE FEATURES.

Method	Val Unseen						Test Unseen					
	Navigation				Grounding		Navigation				Grounding	
	TL	SR ↑	OSR↑	SPL ↑	RGS↑	RGSPL↑	TL	SR ↑	OSR↑	SPL ↑	RGS↑	RGSPL↑
AutoVLN* [9]	-	55.89	62.14	40.85	36.58	26.76	-	55.17	62.30	38.88	32.23	22.68
ScaleVLN* [10]	-	56.97	63.85	41.84	35.76	26.05	-	56.13	62.65	39.52	32.53	22.78
RCM [20]	11.98	9.29	14.23	6.97	4.89	3.89	10.60	7.84	11.68	6.67	3.67	3.14
SMNA [18]	9.07	8.15	11.28	6.44	4.54	3.61	9.23	5.80	8.39	4.53	3.10	2.39
FAST-MATTN [2]	45.28	14.40	28.20	7.19	7.84	4.67	39.05	19.88	30.63	11.60	11.28	6.08
SIA [65]	41.53	31.53	44.67	16.28	22.41	11.56	48.61	30.80	44.56	14.85	19.02	9.20
VLN \odot BERT [36]	16.78	30.67	35.02	24.90	18.77	15.27	15.86	29.61	32.91	23.99	16.50	13.51
Airbert [15]	18.71	27.89	34.51	21.88	18.23	14.18	17.91	30.28	34.20	23.61	16.83	13.28
DUET [39]	22.11	46.98	51.07	33.73	32.15	23.03	21.30	52.51	56.91	36.06	31.88	22.06
KERM [66]	21.85	49.02	53.65	34.83	33.97	24.14	17.32	52.26	57.44	37.46	32.69	23.15
YouTube-VLN [14]	21.87	48.11	53.71	34.43	32.15	23.43	21.94	54.32	60.51	37.34	32.02	21.94
DUET‡ [39] (baseline)	25.64	48.71	53.62	34.26	32.18	22.64	-	-	-	-	-	-
RAM‡(ours)	25.44	51.89	58.47	35.00	34.31	23.20	22.78	57.44	64.26	41.41	36.05	25.77

path. Three other metrics are used for REVERIE: 5) Remote Grounding Success Rate (RGS): the ratio of grounding the correct object when stopping, 6) Remote Grounding Success rate weighted by Path Length (RGSPL): weight RGS by TL, and 7) Oracle Success Rate (OSR): the ratio of containing a viewpoint along the path where the target object is visible. For R4R, we further adopt 8) the Coverage weighted by Length Score (CLS), 9) the normalized Dynamic Time Warping (nDTW), and 10) the Success weighted by nDTW (SDTW) for measuring the path fidelity.

3) *Implementation Details*: We plug our RAM into a powerful pretraining-based baseline [39]. In the pretraining phase, the agent is trained with three proxy tasks: Masked Language Modeling (MLM), Instruction and Trajectory Matching (ITM),

and Single Action Prediction (SAP). In the finetuning phase, the agent is trained with DAGGER [67] method. We add our rewritten data during both the pretraining and finetuning phases to boost the navigation training. The pretraining is conducted for 20k iterations with a batch size of 128 and learning rate of 5e-5 on four NVIDIA RTX 3090 GPUs. Our mixing-then-focusing training strategy is implemented during the finetuning phase, where the maximum training iterations, the batch size, and the learning rate for two stages are set as 20k, 8, and 1e-5, respectively. We resume the best model in stage 1 to train for stage 2. The finetuning is implemented on a single NVIDIA RTX 3090 GPU. The pre-training phase lasts about 50 hours and the fine-tuning phase lasts about 20 hours.

We adopt two kinds of visual encoders, i.e., CLIP ViT B/16 and CLIP ViT L/14 [46] to validate the effectiveness of our method. Like previous works [38], [39], [53], we also add the prevalent data [37] during training. We use Tag2Text [68] as the VLM for observation description collection, and employ ChatGPT [44](with version *gpt-3.5-turbo-1106*) as the LLM for scene description rewriting and instruction rewriting. For an original trajectory-instruction pair, we collect 3 different trajectories containing new panoramas, and for each new trajectory we obtain one corresponding augmentation instruction. The LLMs, VLMs, T2IMs used in the experiments are all in a zero-shot manner without the need for training consumption. The parameter size of our model is 688.51M.

Transfer to Continuous Setting. Following previous works like ScaleVLN [10], we transfer our RAM to the continuous VLN setting by first pretraining the baseline model DUET [39] with both original and our rewritten observation-instruction data on the R2R discrete environments. Then we finetune the pretrained model on R2R-CE based on a pretrained candidate waypoint predictor [59] for a fair comparison with other methods. The finetuning phase is conducted for 30 epochs with a batch size of 8 and a learning rate of 1e-5 on two NVIDIA RTX 3090 GPUs.

B. Comparison with Existing Approaches

R2R. Table II shows the performance comparison of different methods on R2R, where we can find that our RAM using CLIP ViT L/14 features outperforms all previous works that do not introduce large-scale additional data for training like ScaleVLN [10]. Although ScaleVLN outperforms previous works as well as RAM, it resorts to significantly larger realistic data resources ($\times 352$ larger than the R2R dataset) while our RAM only introduces a small scale of generated data ($\times 3$ larger than the R2R dataset). Moreover, our RAM with both two kinds of CLIP features outperforms ScaleVLN [10] in Val Seen split. We can also observe that our RAM outperforms baseline DUET [39] especially in Val Unseen when using both CLIP ViT B/16 and L/14 as image features, revealing its superior generalization ability.

REVERIE. Table III compares different methods regarding the navigation and object grounding performance on REVERIE, where we can find that RAM surpasses the baseline [39] largely on both navigation and object grounding metrics under the same visual features on Val Unseen, e.g., the improvements for SR and RGS are $\sim 3.1\%$ and $\sim 2.2\%$, respectively. RAM also significantly outperforms previous works including AutoVLN [9] and ScaleVLN [10] that introduce large-scale additional simulator data on Test Unseen regarding both navigation and object grounding metrics. These results show that our RAM effectively improves the generalization without the need to introduce large-scale additional realistic data.

R4R. Table IV presents the results on R4R, where RAM outperforms the baseline [39] in both navigation (NE, SR, and SPL) and instruction following (nDTW, sDTW, and CLS) metrics on Val Unseen, showing the effectiveness of our method when facing much longer instructions and trajectories. It is

TABLE IV
PERFORMANCE COMPARISON ON R4R DATASET. ‡: USING CLIP ViT L/14 AS IMAGE FEATURES.

Model	Val Unseen					
	NE↓	SR↑	SPL↑	nDTW↑	sDTW↑	CLS↑
SF [7]	8.47	24	-	-	-	30
RCM [20]	-	29	-	30	13	35
PTA [69]	8.25	24	-	32	10	37
EGP [70]	8.0	30.2	-	37.4	17.5	44.4
DUET-CLIP [53]	6.06	46.61	41.94	-	-	-
PanoGen [53]	6.02	47.78	44.25	-	-	-
DUET‡ [39] (baseline)	5.88	50.35	46.14	40.08	27.91	46.31
RAM‡(ours)	5.18	55.28	49.59	42.05	29.91	47.18

TABLE V
RESULTS ON R2R-CE DATASET. †: USING THE SAME WAYPOINT PREDICTOR [59] FOR A FAIR COMPARISON.

Method	Val Seen			Val Unseen		
	NE↓	OSR↑	SR↑	NE↓	OSR↑	SR↑
CMTF [71]	7.10	45.4	36.1	7.9	38.0	26.4
LAW [72]	6.35	49	40	6.83	44	35
Sim2Sim [73]	4.67	61	52	6.07	52	43
CMA† [59]	5.20	61	51	6.20	52	41
VLN-RecBERT† [59]	5.02	59	50	5.74	53	44
DUET† [39] (baseline)	4.46	62.98	43.32	5.14	59.65	37.25
RAM†(ours)	4.09	65.68	46.92	4.95	61.45	44.15

also superior to a recent data augmentation method [53] that utilizes T2IMs for environment generation based on the original scene description and adopts Speaker-based instruction augmentation. This comparison result shows that our object-enriched observation rewriting strategy can better improve the scene diversity by introducing new objects and spatial layouts. The comparison also demonstrates the superiority of our observation-contrast instruction rewriting scheme over Speaker-based instruction augmentation.

Transfer to R2R-CE. We further transfer our RAM to R2R-CE. As shown in Table V, although our work is mainly established based on discrete environments, it still shows impressive superiority over the baseline method [39] on R2R-CE, revealing its potential to generalize to continuous environments which is more realistic.

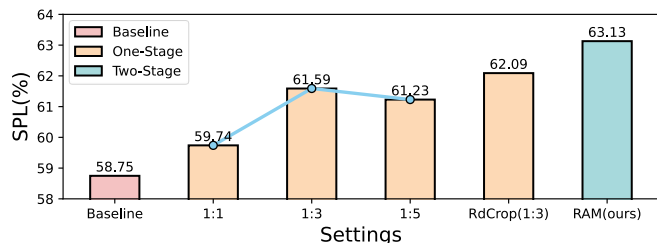


Fig. 4. Ablation results for mixed training strategy on R2R dataset. “1:1”, “1:3”, and “1:5” represent the data mixing ratio between the original human-annotated data and our rewritten data. “RdCrop(1:3)” means using our random observation cropping scheme with the data mixing ratio of 1:3.

TABLE VI

ABLATION RESULTS FOR OBSERVATION-INSTRUCTION REWRITING. ‘‘PAN’’ STANDS FOR GENERATED PANORAMIC IMAGES, ‘‘DES.’’ MEANS REWRITTEN OBJECT-ENRICHED SCENE DESCRIPTIONS, AND ‘‘INS.’’ MEANS REWRITTEN INSTRUCTIONS, RESPECTIVELY.

No.	Settings			Val Seen		Val Unseen	
	Pan.	Des.	Ins.	NE ↓	SR ↑	NE ↓	SR ↑
Baseline	✗	✗	✗	2.91	74.73	3.70	65.94
speaker inst	✗	✗	✗	3.19	70.91	3.83	65.05
1	✓	✗	✗	2.76	74.14	3.54	67.52
2	✗	✗	✓	2.76	74.83	3.66	67.43
3	✓	✗	✓	2.66	74.34	3.51	68.08
4	✓	✓	✗	2.44	77.08	3.50	69.69
5	✓	✓	✓	2.37	78.55	3.42	70.29

TABLE VII

ABLATION RESULTS OF ADDING DATA AUGMENTED VIA RAM IN DIFFERENT TRAINING PHASES ON R2R.

No.	Settings		Val Seen		Val Unseen	
	Pretraining	Finetuning	SR ↑	SPL ↑	SR ↑	SPL ↑
Baseline	✗	✗	80.80	73.64	72.37	58.75
1	✓	✗	80.71	75.08	71.99	62.32
2	✗	✓	80.71	74.56	73.61	62.46
3	✓	✓	82.17	77.70	73.65	63.13

C. Ablation Study

We conduct ablation studies to analyze the effects of different method components and the impacts of adding our augmentation data during different training phases. We use CLIP ViT B/16 features for the ablation experiments. For the baseline in Table II, Fig. 4, and Table VII, we reproduce the baseline model DUET [39] with CLIP ViT B/16 visual features. In Table VI, since we aim to verify the effectiveness of our rewritten data and exclude the effect of high-quality human annotated instructions, we train the baseline using the widely used R2R augmentation dataset [74], which can provide a fair comparison of different kinds of augmentation data.

Effectiveness of Observation-Instruction Rewriting. Table VI presents the ablation results of our observation-instruction rewriting, where we can draw the following crucial conclusions: (1) By comparing No.1~No.5 with the baseline and speaker inst, we can find that both our rewritten observations and instructions augmented by RAM are helpful for increasing the diversity of training data, leading to large performance improvement. For example, No.1 and No.2 which perform solely observation or instruction rewriting have already outperformed the Baseline. Moreover, No.5 with both rewriting procedures achieves the best performance. (2) The comparison between No.1 and No.4 shows the effectiveness of object-enriched description rewriting that generating observations based on the rewritten scene descriptions brings larger performance enhancement than that based on the original scene description. (3) The superior performance of No.5 compared to No.3 (Pan. & Ins.) indicates that our object-enriched observation rewriting scheme effectively enhances observation diversity through the object-enriched scene description rewriting strategy (denoted as ‘‘Des.’’), thereby leading to significant

TABLE VIII

COMPARISON WITH THE BASELINE METHOD [39] UNDER THE LOW-RESOURCE SETTINGS. USING CLIP ViT B/16 AS IMAGE FEATURES.

Model	Val Unseen					
	20%		40%		60%	
	NE↓	SR↑	NE↓	SR↑	NE↓	SR↑
Baseline [39]	3.58	68.03	3.26	71.05	3.43	69.39
RAM (ours)	3.36	70.80	3.19	71.99	3.19	72.71

performance improvements. (4) No.2 significantly outperforms speaker inst that using Speaker-augmented instructions, revealing that our rewritten instructions are more informative and diverse, which are beneficial for improving the cross-modal alignment ability of the VLN agent.

Effectiveness of Mixing-then-Focusing Training Mechanism. Fig. 4 presents the ablation results for different data fusion strategies for finetuning training. The results of RAM vs. one-stage variant (denoted as 1:1, 1:3, 1:5) sufficiently show the effectiveness of our mixing-then-focusing training strategy. The improvement of RdCrop (1:3) over ‘‘1:3’’ further shows the effectiveness of our random observation cropping scheme that mitigates the noise brought by the foundation models and improves the data distribution diversity. Moreover, by comparing mixing training with different proportions of rewritten data (1:1, 1:3, 1:5), we can find that simply adding more rewritten data may not contribute to linear performance improvement. This reveals the importance of exploring effective data fusion mechanisms for activating the advantage of augmentation data, and our mixing-then-focusing training strategy can inspire future research for this.

Pretraining & Finetuning Ablation Results. Table VII gives the ablation results of adding RAM augmentation data in different training phases. For No.1 in Table VII, we directly mix the original data with our rewritten data in the pretraining phase, and then finetune the model using only the original data. For No.2 in Table VII, we conduct the pretraining following the baseline model using original data, and then implement our mixing-then-focusing training mechanism using both original and rewritten data in the finetuning phase. In Table VII, through the comparison between the Baseline and No.2, we can find that adding our RAM data during the finetuning phase can effectively improve the navigation performance in Val Unseen, showing that our augmentation data is helpful for improving the generalization ability of the VLN agent to unseen scenarios. Moreover, No.3 shows that by further adding our augmentation data in the pretraining phase, the metric results under both Val Seen and Val Unseen can be further boosted. These results show the positive impact of our RAM for enhancing training in different training phases.

D. Low-Resource Experiments

We further conduct a low-resource experiment to verify how our RAM augmentation data can help mitigate the data scarcity issue. To this end, we only extract partial original data for the training of Baseline [39]. Concretely, we randomly extract the data at different proportions and there may be large distributional discrepancies among extracted training subsets



Fig. 5. Visualization examples of rewritten object-enriched scene descriptions, generated panorama, extracted ground-truth sequence from the generated panorama, and the rewritten instruction. Generated new scene objects and modality-aligned objects in instructions are denoted in red and blue fonts/boxes, respectively.



Fig. 6. Visualization comparison of instructions generated by the Speaker model [53] and our RAM. Modality-aligned objects in the instruction are denoted in blue fonts/boxes.

at different proportions. For RAM, we add our rewritten data augmented from the corresponding partial original data. From Table VIII we can find that our RAM surpasses the baseline when extracting original data with different proportions. Especially, our RAM achieves comparable performance to the baseline which uses total original training data in Table VII under the 60% setting. An interesting phenomenon we can also find in Table VIII is that the baseline appears to generalize better with 40% data compared to 60%, which may be caused by large distributional discrepancies among extracted training subsets at different ratios. Moreover, it is also reasonable since it is common that the relationship between performance improvements and data scale is not linear, as also be demonstrated in Fig. 4 for our augmentation data scale ablation.

These results further show the practicality of our RAM in real-world applications where the manually annotated data is usually limited.

E. Visualization

Rewritten Observation-Instruction Examples. Fig. 5 presents a visualization example of rewritten data by our RAM. From the rewritten object-enriched descriptions generated by the LLM, we can find that diverse objects, e.g., *armchair* and *coffee table*, are indicated explicitly. Benefiting from it, the panorama generated by the T2IM contains these newly introduced objects with new spatial layouts, leading to great diversity enhancement of the environment. Moreover, we can observe that the extracted single-view images are also



Fig. 7. Candidate observations for three consecutive steps. The cross-step semantically consisting objects are denoted in fonts/boxes in the same color.

high-quality compared to the images taken by the camera in Matterport3D dataset. We can also find that the rewritten instruction successfully indicates modality-aligned objects, e.g., *hallway* and *plants* in the new trajectory, revealing the effectiveness of our observation-contrast instruction rewriting.

Comparison between Speaker-based instructions and RAM instructions. We further give a visualization comparison of instructions generated by the Speaker model [53] and our RAM in Fig. 6, where we can find the instruction generated through the Speaker model is less informative, e.g. it contains repeated phrases “walk around the table and chairs”. We can also observe that the instruction does not align well with the observations, e.g., the observations do not contain the *table* mentioned in the instruction, and the generated instruction changes the original actional information “turn right” to the wrong action “turn left”. In contrast, the rewritten instruction by our RAM introduces reasonable actional representations as well as indicates multiple modality-aligned objects (such as *small kitchen* and *hammock*) that are different from those in the original instruction, which can effectively improve the cross-modal alignment ability of the agent.

Cross-step Consistency. We also give the visualization of candidate observations for multiple consecutive steps extracted from our rewritten panoramas in Fig. 7, to study whether our rewritten observations can capture cross-step consistency. Since we use Text-to-Image Generation models (T2IMs) to generate rewritten panoramas for each step separately, there is no explicit constraint to ensure absolute cross-step observation overlap in our RAM. However, since our scene description rewriting mechanism can essentially generate or retain some consistent object categories for the same scene appearing in consecutive navigation timesteps, the generated panoramas can therefore have cross-step semantic consistency. For example, the *potted plant* can be observed in both B in Step 2 and C in Step 3. Such cross-step semantic consistency can contribute to reasonable sequential action decisions, and our introduced rewritten data has also proved to be helpful for enhancing navigation performance from extensive experimental results.

V. CONCLUSION

In this work, we propose a novel rewriting-driven augmentation (RAM) paradigm for the VLN task, where we create unseen observation-instruction pairs via performing object-enriched observation rewriting and observation-contrast instruction rewriting. Our RAM fulfills simulator-free and labor-saving data augmentation, powered by delicate collaboration

of various foundation models. We also introduce a mixing-then-focusing strategy accompanied by a random observation cropping scheme for boosting training with our rewritten data. Experimental results exhibit the impressive generalization ability of RAM on multiple popular VLN benchmarks. We believe our work can provide new insights for how to create and leverage augmentation data to address the critical data scarcity issue in embodied tasks. In the future, we would like to introduce more effective mechanisms like parameter-efficient finetuning and feedback-based learning to further adapt foundation models for VLN data augmentation.

REFERENCES

- [1] P. Anderson, Q. Wu, D. Teney, J. Bruce, M. Johnson, N. Sunderhauf, I. Reid, S. Gould, and A. van den Hengel, “Vision-and-language navigation: Interpreting visually-grounded navigation instructions in real environments,” in *Proceedings of the IEEE Conference on Computer Vision and Pattern Recognition (CVPR)*, 2018.
- [2] Y. Qi, Q. Wu, P. Anderson, X. Wang, W. Y. Wang, C. Shen, and A. van den Hengel, “Reverie: Remote embodied visual referring expression in real indoor environments,” in *Proceedings of the IEEE Conference on Computer Vision and Pattern Recognition (CVPR)*, 2020.
- [3] A. Ku, P. Anderson, R. Patel, E. Ie, and J. Baldrige, “Room-across-room: Multilingual vision-and-language navigation with dense spatiotemporal grounding,” in *Proceedings of the Conference on Empirical Methods in Natural Language Processing (EMNLP)*, 2020.
- [4] J. Thomason, M. Murray, M. Cakmak, and L. Zettlemoyer, “Vision-and-dialog navigation,” in *Proceedings of the Conference on Robot Learning (CoRL)*, 2019.
- [5] A. Chang, A. Dai, T. Funkhouser, M. Halber, M. Niessner, M. Savva, S. Song, A. Zeng, and Y. Zhang, “Matterport3d: Learning from rgb-d data in indoor environments,” *arXiv preprint arXiv:1709.06158*, 2017.
- [6] H. Tan, L. Yu, and M. Bansal, “Learning to navigate unseen environments: Back translation with environmental dropout,” in *NAACL-HLT*, 2019.
- [7] D. Fried, R. Hu, V. Cirik, A. Rohrbach, J. Andreas, L.-P. Morency, T. Berg-Kirkpatrick, K. Saenko, D. Klein, and T. Darrell, “Speaker-follower models for vision-and-language navigation,” in *Proceedings of the Conference on Neural Information Processing Systems (NeurIPS)*, 2018.
- [8] C. Liu, F. Zhu, X. Chang, X. Liang, Z. Ge, and Y.-D. Shen, “Vision-language navigation with random environmental mixup,” in *Proceedings of the IEEE International Conference on Computer Vision (ICCV)*, 2021.
- [9] S. Chen, P.-L. Guhur, M. Tapaswi, C. Schmid, and I. Laptev, “Learning from unlabeled 3d environments for vision-and-language navigation,” in *Proceedings of the European Conference on Computer Vision (ECCV)*. Springer, 2022, pp. 638–655.
- [10] Z. Wang, J. Li, Y. Hong, Y. Wang, Q. Wu, M. Bansal, S. Gould, H. Tan, and Y. Qiao, “Scaling data generation in vision-and-language navigation,” in *Proceedings of the IEEE International Conference on Computer Vision (ICCV)*, 2023.
- [11] T.-J. Fu, X. E. Wang, M. F. Peterson, S. T. Grafton, M. P. Eckstein, and W. Y. Wang, “Counterfactual vision-and-language navigation via adversarial path sampler,” in *Proceedings of the European Conference on Computer Vision (ECCV)*, 2020.
- [12] S. K. Ramakrishnan, A. Gokaslan, E. Wijmans, O. Maksymets, A. Clegg, J. Turner, E. Undersander, W. Galuba, A. Westbury, A. X. Chang *et al.*, “Habitat-matterport 3d dataset (hm3d): 1000 large-scale 3d environments for embodied ai,” *arXiv preprint arXiv:2109.08238*, 2021.
- [13] F. Xia, A. R. Zamir, Z. He, A. Sax, J. Malik, and S. Savarese, “Gibson env: Real-world perception for embodied agents,” in *Proceedings of the IEEE Conference on Computer Vision and Pattern Recognition (CVPR)*, 2018, pp. 9068–9079.
- [14] K. Lin, P. Chen, D. Huang, T. H. Li, M. Tan, and C. Gan, “Learning vision-and-language navigation from youtube videos,” in *Proceedings of the IEEE International Conference on Computer Vision (ICCV)*, 2023, pp. 8317–8326.
- [15] P.-L. Guhur, M. Tapaswi, S. Chen, I. Laptev, and C. Schmid, “Airbert: In-domain pretraining for vision-and-language navigation,” in *Proceedings of the IEEE International Conference on Computer Vision (ICCV)*, 2021.

- [16] V. Jain, G. Magalhaes, A. Ku, A. Vaswani, E. Je, and J. Baldridge, “Stay on the path: Instruction fidelity in vision-and-language navigation,” in *Proceedings of the Association for Computational Linguistics (ACL)*, 2019.
- [17] J. Krantz, E. Wijmans, A. Majumdar, D. Batra, and S. Lee, “Beyond the nav-graph: Vision-and-language navigation in continuous environments,” in *Computer Vision—ECCV 2020: 16th European Conference, Glasgow, UK, August 23–28, 2020, Proceedings, Part XXVIII 16*. Springer, 2020, pp. 104–120.
- [18] C.-Y. Ma, Jiasen lu, Z. Wu, G. AlRegib, Z. Kira, richard socher, and C. Xiong, “Self-monitoring navigation agent via auxiliary progress estimation,” in *Proceedings of the International Conference on Learning Representations (ICLR)*, 2019.
- [19] Y. Qi, Z. Pan, S. Zhang, A. van den Hengel, and Q. Wu, “Object-and-action aware model for visual language navigation,” in *Proceedings of the European Conference on Computer Vision (ECCV)*, 2020.
- [20] X. Wang, Q. Huang, A. Celikyilmaz, J. Gao, D. Shen, Y.-F. Wang, W. Y. Wang, and L. Zhang, “Reinforced cross-modal matching and self-supervised imitation learning for vision-language navigation,” in *Proceedings of the IEEE Conference on Computer Vision and Pattern Recognition (CVPR)*, 2019.
- [21] F. Zhu, Y. Zhu, X. Chang, and X. Liang, “Vision-language navigation with self-supervised auxiliary reasoning tasks,” in *Proceedings of the IEEE Conference on Computer Vision and Pattern Recognition (CVPR)*, 2020.
- [22] H. Wang, Q. Wu, and C. Shen, “Soft expert reward learning for vision-and-language navigation,” in *Proceedings of the European Conference on Computer Vision (ECCV)*, 2020.
- [23] T. Wang, Z. Wu, and D. Wang, “Visual perception generalization for vision-and-language navigation via meta-learning,” *IEEE Transactions on Neural Networks and Learning Systems*, vol. 34, no. 8, pp. 5193–5199, 2021.
- [24] B. Lin, Y. Long, Y. Zhu, F. Zhu, X. Liang, Q. Ye, and L. Lin, “Towards deviation-robust agent navigation via perturbation-aware contrastive learning,” *IEEE Transactions on Pattern Analysis and Machine Intelligence*, vol. 45, no. 10, pp. 12 535–12 549, 2023.
- [25] X. Shu, B. Xu, L. Zhang, and J. Tang, “Multi-granularity anchor-contrastive representation learning for semi-supervised skeleton-based action recognition,” *IEEE Transactions on Pattern Analysis and Machine Intelligence*, vol. 45, no. 6, pp. 7559–7576, 2023.
- [26] X. Liang, F. Zhu, Y. Zhu, B. Lin, B. Wang, and X. Liang, “Contrastive instruction-trajectory learning for vision-language navigation,” in *Proceedings of the AAAI Conference on Artificial Intelligence*, vol. 36, no. 2, 2022, pp. 1592–1600.
- [27] B. Lin, Y. Zhu, Y. Long, X. Liang, Q. Ye, and L. Lin, “Adversarial reinforced instruction attacker for robust vision-language navigation,” *IEEE Transactions on Pattern Analysis and Machine Intelligence*, vol. 44, no. 10, pp. 7175–7189, 2021.
- [28] J. Wang, T. Wang, L. Xu, Z. He, and C. Sun, “Discovering intrinsic subgoals for vision-and-language navigation via hierarchical reinforcement learning,” *IEEE Transactions on Neural Networks and Learning Systems*, pp. 1–13, 2024.
- [29] L. Xie, M. Zhang, Y. Li, W. Qin, Y. Yan, and E. Yin, “Vision–language navigation with beam-constrained global normalization,” *IEEE Transactions on Neural Networks and Learning Systems*, vol. 35, no. 1, pp. 1352–1363, 2024.
- [30] T. Wang, Z. Wu, and D. Wang, “Visual perception generalization for vision-and-language navigation via meta-learning,” *IEEE Transactions on Neural Networks and Learning Systems*, vol. 34, no. 8, pp. 5193–5199, 2023.
- [31] G. Li, N. Duan, Y. Fang, M. Gong, and D. Jiang, “Unicoder-vl: A universal encoder for vision and language by cross-modal pre-training,” in *Proceedings of the Association for the Advance of Artificial Intelligence (AAAI)*, 2020.
- [32] X. Li, X. Yin, C. Li, P. Zhang, X. Hu, L. Zhang, L. Wang, H. Hu, L. Dong, F. Wei, Y. Choi, and J. Gao, “Oscar: Object-semantics aligned pre-training for vision-language tasks,” in *Proceedings of the European Conference on Computer Vision (ECCV)*, 2020.
- [33] Y.-C. Chen, L. Li, L. Yu, A. E. Kholý, F. Ahmed, Z. Gan, Y. Cheng, and J. Liu, “Uniter: Universal image-text representation learning,” in *Proceedings of the European Conference on Computer Vision (ECCV)*, 2020.
- [34] J. Lu, D. Batra, D. Parikh, and S. Lee, “Vilbert: Pretraining task-agnostic visiolinguistic representations for vision-and-language tasks,” in *Proceedings of the Conference on Neural Information Processing Systems (NeurIPS)*, 2019.
- [35] L. H. Li, M. Yatskar, D. Yin, C.-J. Hsieh, and K.-W. Chang, “Visualbert: A simple and performant baseline for vision and language,” *arXiv preprint arXiv:1908.03557*, 2019.
- [36] Y. Hong, Q. Wu, Y. Qi, C. Rodriguez-Opazo, and S. Gould, “Vln bert: A recurrent vision-and-language bert for navigation,” in *Proceedings of the IEEE Conference on Computer Vision and Pattern Recognition (CVPR)*, 2021.
- [37] W. Hao, C. Li, X. Li, L. Carin, and J. Gao, “Towards learning a generic agent for vision-and-language navigation via pre-training,” in *Proceedings of the IEEE Conference on Computer Vision and Pattern Recognition (CVPR)*, 2020.
- [38] S. Chen, P.-L. Guhur, C. Schmid, and I. Laptev, “History aware multi-modal transformer for vision-and-language navigation,” in *Proceedings of the Conference on Neural Information Processing Systems (NeurIPS)*, 2021.
- [39] S. Chen, P.-L. Guhur, M. Tapaswi, C. Schmid, and I. Laptev, “Think global, act local: Dual-scale graph transformer for vision-and-language navigation,” in *Proceedings of the IEEE Conference on Computer Vision and Pattern Recognition (CVPR)*, 2022.
- [40] D. An, Y. Qi, Y. Li, Y. Huang, L. Wang, T. Tan, and J. Shao, “Bebert: Multimodal map pre-training for language-guided navigation,” in *Proceedings of the IEEE International Conference on Computer Vision (ICCV)*, 2023, pp. 2737–2748.
- [41] Y. Zhao, J. Chen, C. Gao, W. Wang, L. Yang, H. Ren, H. Xia, and S. Liu, “Target-driven structured transformer planner for vision-language navigation,” in *Proceedings of the ACM International Conference on Multimedia (ACM MM)*, 2022.
- [42] Y. Qi, Z. Pan, Y. Hong, M.-H. Yang, A. van den Hengel, and Q. Wu, “The road to know-where: An object-and-room informed sequential bert for indoor vision-language navigation,” in *Proceedings of the IEEE International Conference on Computer Vision (ICCV)*, 2021.
- [43] S. Tan, K. Sima, D. Wang, M. Ge, D. Guo, and H. Liu, “Self-supervised 3-d semantic representation learning for vision-and-language navigation,” *IEEE Transactions on Neural Networks and Learning Systems*, 2024.
- [44] OpenAI, “Introducing chatgpt,” <https://openai.com/blog/chatgpt>, 2022.
- [45] O. OpenAI, “Gpt-4 technical report,” Mar 2023.
- [46] A. Radford, J. W. Kim, C. Hallacy, A. Ramesh, G. Goh, S. Agarwal, G. Sastry, A. Askell, P. Mishkin, J. Clark, G. Krueger, and I. Sutskever, “Learning transferable visual models from natural language supervision,” in *Proceedings of the International Conference on Machine Learning (ICML)*, 2021.
- [47] W. Dai, J. Li, D. Li, A. Tiong, J. Zhao, W. Wang, B. Li, P. Fung, and S. Hoi, “Instructblip: Towards general-purpose vision-language models with instruction tuning. arxiv 2023,” *arXiv preprint arXiv:2305.06500*, vol. 2, 2023.
- [48] G. Zhou, Y. Hong, and Q. Wu, “Navgpt: Explicit reasoning in vision-and-language navigation with large language models,” in *AAAI*, 2024.
- [49] Y. Long, X. Li, W. Cai, and H. Dong, “Discuss before moving: Visual language navigation via multi-expert discussions,” *arXiv preprint arXiv:2309.11382*, 2023.
- [50] J. Chen, B. Lin, R. Xu, Z. Chai, X. Liang, and K.-Y. Wong, “Mapgpt: Map-guided prompting with adaptive path planning for vision-and-language navigation,” in *Proceedings of the 62nd Annual Meeting of the Association for Computational Linguistics (Volume 1: Long Papers)*, 2024, pp. 9796–9810.
- [51] B. Lin, Y. Nie, Z. Wei, Y. Zhu, H. Xu, S. Ma, J. Liu, and X. Liang, “Correctable landmark discovery via large models for vision-language navigation,” *IEEE Transactions on Pattern Analysis and Machine Intelligence*, 2024.
- [52] J. Li, H. Tan, and M. Bansal, “Envedit: Environment editing for vision-and-language navigation,” in *Proceedings of the IEEE Conference on Computer Vision and Pattern Recognition (CVPR)*, 2022.
- [53] J. Li and M. Bansal, “Panogen: Text-conditioned panoramic environment generation for vision-and-language navigation,” in *Proceedings of the Conference on Neural Information Processing Systems (NeurIPS)*, 2024.
- [54] T. Xiao, H. Chan, P. Sermanet, A. Wahid, A. Brohan, K. Hausman, S. Levine, and J. Tompson, “Robotic skill acquisition via instruction augmentation with vision-language models,” *arXiv preprint arXiv:2211.11736*, 2022.
- [55] L. Wang, Y. Ling, Z. Yuan, M. Shridhar, C. Bao, Y. Qin, B. Wang, H. Xu, and X. Wang, “Gensim: Generating robotic simulation tasks via large language models,” *arXiv preprint arXiv:2310.01361*, 2023.
- [56] Y. Yang, F.-Y. Sun, L. Weihs, E. Vanderbilt, A. Herrasti, W. Han, J. Wu, N. Haber, R. Krishna, L. Liu *et al.*, “Holodeck: Language guided generation of 3d embodied ai environments,” in *Proceedings of the IEEE Conference on Computer Vision and Pattern Recognition (CVPR)*, 2024.

- [57] Y. Wang, Z. Xian, F. Chen, T.-H. Wang, Y. Wang, K. Fragkiadaki, Z. Erickson, D. Held, and C. Gan, “Robogen: Towards unleashing infinite data for automated robot learning via generative simulation,” *arXiv preprint arXiv:2311.01455*, 2023.
- [58] A. Zala, J. Cho, H. Lin, J. Yoon, and M. Bansal, “Envgen: Generating and adapting environments via llms for training embodied agents,” *arXiv preprint arXiv:2403.12014*, 2024.
- [59] Y. Hong, Z. Wang, Q. Wu, and S. Gould, “Bridging the gap between learning in discrete and continuous environments for vision-and-language navigation,” in *Proceedings of the IEEE/CVF Conference on Computer Vision and Pattern Recognition*, 2022, pp. 15 439–15 449.
- [60] O. Bar-Tal, L. Yariv, Y. Lipman, and T. Dekel, “Multidiffusion: Fusing diffusion paths for controlled image generation,” in *Proceedings of the International Conference on Machine Learning (ICML)*, 2023.
- [61] D. Shah, B. Osinski, B. Ichter, and S. Levine, “Lm-nav: Robotic navigation with large pre-trained models of language, vision, and action,” in *Proceedings of the Conference on Robot Learning (CoRL)*, 2022.
- [62] Z. Cai, M. Mueller, R. Birkl, D. Wofk, S. Tseng, J. Cheng, G. B.-M. Stan, V. Lal, and M. Paulitsch, “L-magic: Language model assisted generation of images with coherence,” *ArXiv*, vol. abs/2406.01843, 2024. [Online]. Available: <https://api.semanticscholar.org/CorpusID:270226656>
- [63] M. Savva, A. Kadian, O. Maksymets, Y. Zhao, E. Wijnmans, B. Jain, J. Straub, J. Liu, V. Koltun, J. Malik *et al.*, “Habitat: A platform for embodied ai research,” in *Proceedings of the IEEE/CVF international conference on computer vision*, 2019, pp. 9339–9347.
- [64] Y. Qiao, Y. Qi, Y. Hong, Z. Yu, P. Wang, and Q. Wu, “Hop: History-and-order aware pre-training for vision-and-language navigation,” in *Proceedings of the IEEE Conference on Computer Vision and Pattern Recognition (CVPR)*, 2022.
- [65] X. Lin, G. Li, and Y. Yu, “Scene-intuitive agent for remote embodied visual grounding,” in *Proceedings of the IEEE Conference on Computer Vision and Pattern Recognition (CVPR)*, 2021.
- [66] X. Li, Z. Wang, J. Yang, Y. Wang, and S. Jiang, “Kerm: Knowledge enhanced reasoning for vision-and-language navigation,” in *Proceedings of the IEEE Conference on Computer Vision and Pattern Recognition (CVPR)*, 2023.
- [67] S. Ross, G. Gordon, and D. Bagnell, “A reduction of imitation learning and structured prediction to no-regret online learning,” in *Proceedings of the fourteenth international conference on artificial intelligence and statistics. JMLR Workshop and Conference Proceedings*, 2011, pp. 627–635.
- [68] X. Huang, Y. Zhang, J. Ma, W. Tian, R. Feng, Y. Zhang, Y. Li, Y. Guo, and L. Zhang, “Tag2text: Guiding vision-language model via image tagging,” *arXiv preprint arXiv:2303.05657*, 2023.
- [69] F. Landi, L. Baraldi, M. Cornia, M. Corsini, and R. Cucchiara, “Perceive, transform, and act: Multi-modal attention networks for vision-and-language navigation,” *ArXiv*, vol. abs/1911.12377, 2019.
- [70] Z. Deng, K. Narasimhan, and O. Russakovsky, “Evolving graphical planner: Contextual global planning for vision-and-language navigation,” in *Proceedings of the Conference on Neural Information Processing Systems (NeurIPS)*, 2020.
- [71] K. Chen, J. K. Chen, J. Chuang, M. Vázquez, and S. Savarese, “Topological planning with transformers for vision-and-language navigation,” in *Proceedings of the IEEE/CVF Conference on Computer Vision and Pattern Recognition*, 2021, pp. 11 276–11 286.
- [72] S. Raychaudhuri, S. Wani, S. Patel, U. Jain, and A. Chang, “Language-aligned waypoint (law) supervision for vision-and-language navigation in continuous environments,” in *Proceedings of the 2021 Conference on Empirical Methods in Natural Language Processing*, 2021, pp. 4018–4028.
- [73] J. Krantz and S. Lee, “Sim-2-sim transfer for vision-and-language navigation in continuous environments,” in *European Conference on Computer Vision*. Springer, 2022, pp. 588–603.
- [74] W. Hao, C. Li, X. Li, L. Carin, and J. Gao, “Towards learning a generic agent for vision-and-language navigation via pre-training,” in *Proceedings of the IEEE Conference on Computer Vision and Pattern Recognition (CVPR)*, 2020.
- [75] J. Li, D. Li, C. Xiong, and S. Hoi, “Blip: Bootstrapping language-image pre-training for unified vision-language understanding and generation,” in *International conference on machine learning*. PMLR, 2022, pp. 12 888–12 900.
- [76] H. Liu, C. Li, Q. Wu, and Y. J. Lee, “Visual instruction tuning,” in *NeurIPS*, 2023.

Supplementary Materials

I. METHOD DETAILS

To improve readability and clarity, we provide pseudocodes for our mixing-then-focusing strategy and the data augmentation pipeline, presented in Algorithm 1 and Algorithm 2 on the last page, respectively.

II. IMPLEMENTATION DETAILS

A. Scale of augmented data

For each dataset R2R, REVERIE, and R4R, the augmentation data are 3 times larger than the original dataset, shown in Table IX, which is significantly smaller than other methods such as AutoVLN [9] and ScaleVLN [10]. All our augmentation data are utilized in both pretraining and finetuning phases.

TABLE IX
SCALE OF AUGMENTED DATA FOR OUR RAM AND SCALEVLN [10].

Dataset	R2R & R4R (ours)	REVERIE (ours)	R2R (ScaleVLN)
Amount of Augmented Data	14,025	12,450	4,941,710

B. Choices of foundation models and implementation details

For generating observations, the reason for selecting Multidiffusion [60] as the T2I model used in our pipeline has been indicated in our original manuscript, i.e., the Multidiffusion model is more suitable for generating panoramas. In the original Multidiffusion [60] paper, the authors have also demonstrated its superior capability of panorama generation over Stable Diffusion.

For generating scene descriptions, we have compared the descriptions obtained through different popular VLMs, including BLIP [75], Tag2text [68], and LLaVA [76], and chose Tag2Text [68] finally since it tends to capture informative and salient objects in the observation image. We also put a comparison visualization example here in Fig. 8. The results in Fig. 8 reveal that BLIP tends to miss critical objects in the scene and LLaVA often generates redundant or irrelevant information for image generation. In contrast, Tag2text can accurately identify noteworthy objects and generate informative captions.

Regarding the choice of LLM, we selected *gpt-3.5-turbo-1106* by considering its low cost and satisfactory performance. While more advanced and expensive LLMs, such as GPT-4, might generate better scene descriptions, it may be constrained by the marginal benefit of performance improvements.

The VLM, LLM, and T2IM used in our data augmentation pipeline are all employed in an off-the-shelf manner. For the VLM (i.e., Tag2text [68]), we keep the original parameter setting (e.g. *threshold for tagging* and *input image size*) for obtaining scene descriptions. For LLM (i.e., ChatGPT [44]), we set the parameter *temperature* to 0.8 and *presence_penalty* to 0. For the T2IM (i.e., Multidiffusion [60]), we fix the parameter *num_inference_steps* of the MultiDiffusion model to 30 for generating panoramas with high quality and resolution in a tolerable time consumption.

C. Details on the time, computational cost and resources

Details on the time, computational cost, and resources required for generating the augmented data by our RAM is presented in Table X. Concretely, we utilized VLM and T2I models to obtain observation descriptions and augmented observations on 8 NVIDIA RTX 3090 GPUs by splitting data into plenty of batches in 1 hour and 30 hours, respectively. Rewritten observation descriptions and rewritten instructions were collected by querying LLMs within 30 minutes. Overall, the entire data augmentation pipeline requires less than ~ 2 days and relatively low computational resources.

III. MORE EXPERIMENTS AND VISUALIZATION

A. Performance comparison with baseline HAMT on R2R

We have incorporated a new baseline, HAMT [38], along with corresponding experiments on the R2R dataset, as presented in Table XI here. From Table XI, we can observe that our RAM outperforms the baseline HAMT in both Val Seen and Val Unseen, e.g. it brings $\sim 3\%$ improvements in SPL in Val Unseen. The results on different baselines sufficiently show the effectiveness and generalization ability of our proposed method.

B. Comparison with ScaleVLN on the same data scale

Table XII shows a new ablation experiment with CLIP VIT B/16 visual features. Considering that acquiring data at the scale of ScaleVLN [10] is highly labor-intensive and poses significant storage challenges, we conduct an alternative experimental comparison between ScaleVLN [10] and our RAM. Specifically, we train DUET [39] agent using the ScaleVLN data with the same amount of augmented data as our RAM, i.e., we randomly sample 14,025 trajectory-instruction pairs (x3 times the data amount of the original R2R data) from the ScaleVLN [10] dataset in R2R dataset². We have presented the result here in Table XII. From Table XII, we can observe that the “DUET+ScaleVLN(subset)” setting surpasses the baseline, yet its performance is inferior to that of our RAM. Moreover, this setting’s performance on the Val Seen drops by approximately $\sim 6\%$ in SR and $\sim 8\%$ in SPL compared to the baseline, which may be attributed to the introduction of a large amount of unfamiliar real-world simulator data causing the agent to lose its generalization capacity in the original simulation environment. Additionally, we can see that our RAM outperforms ScaleVLN in Val Unseen with the same data scale, which further validates the high quality of our augmented data and the effectiveness of our proposed mixed training mechanism.

C. Comparison with object deletion

To realize object deletion, we mask some specific objects in the observations following EnvEdit [52] and remove the corresponding objects from the rewritten instructions. We present the results here in Table XIII, where we can find that

²The CLIP VIT B/16 visual features are provided by the ScaleVLN GitHub repository, <https://github.com/wz0919/ScaleVLN>.

TABLE X
 DETAILS ON THE TIME, COMPUTATIONAL COST, AND RESOURCES REQUIRED FOR GENERATING THE AUGMENTED DATA BY OUR RAM.

No.	Data Collection Process	Foundation Models	API Querying	Money Cost	GPUs	Time Consumption
1	Observation Descriptions	VLM	✗	-	✓	< 1 hours
2	Rewritten Observation Descriptions	LLM	✓	10 dollars	✗	< 30 minutes
3	Augmented Observations	T2I Model	✗	-	✓	~ 30 hours
4	Rewritten Instructions	LLM	✓	10 dollars	✗	< 30 minutes

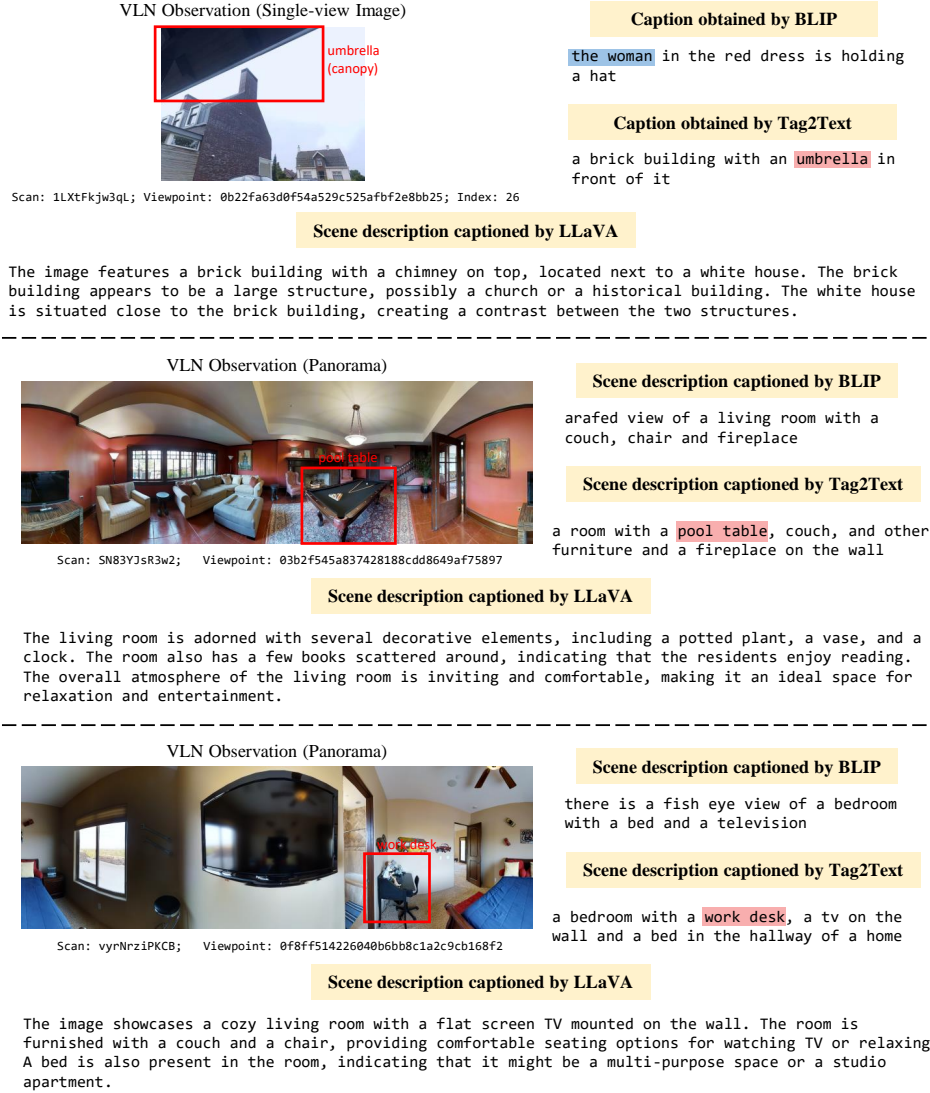


Fig. 8. Captions of single-view images and Scene descriptions of panoramas obtained by different VLMs [68], [75]. Scene objects are denoted in red fonts/boxes, and the wrong noun in the caption is denoted in blue box.

TABLE XI
 COMPARISON RESULTS WITH THE BASELINE HAMT [38] ON R2R DATASET. †: USING CLIP ViT B/16 AS IMAGE FEATURES.

Method	Val Seen				Val Unseen			
	TL	NE ↓	SR ↑	SPL ↑	TL	NE ↓	SR ↑	SPL ↑
HAMT† [38] (baseline)	11.80	3.08	70.52	66.80	12.06	4.09	62.03	56.62
HAMT+RAM† (ours)	10.94	2.82	73.95	71.11	11.45	3.91	63.26	59.27

TABLE XII
 COMPARISON WITH BASELINE METHOD [39] AND SCALEVLN [10] WITH THE SAME SCALE AS OURS (X3 TIMES LARGER THAN THE R2R DATASET). †: USING CLIP ViT B/16 AS VISUAL FEATURES.

Method	Val Seen				Val Unseen			
	TL	NE ↓	SR ↑	SPL ↑	TL	NE ↓	SR ↑	SPL ↑
DUET† [39] (baseline)	13.86	2.12	80.80	73.64	16.22	3.06	72.37	58.75
DUET+ScaleVLN(subset)†	13.84	2.75	74.14	65.62	13.67	3.11	73.01	62.60
DUET+RAM† (ours)	11.50	1.95	82.17	77.70	13.33	2.96	73.65	63.13

object deletion can also improve performance, indicating that this approach is another effective way to generate meaningful augmented data. It provides a valuable reference for designing future data augmentation approaches. Furthermore, the results in Table XIII show that our RAM outperforms

the object deletion, suggesting that introducing a greater variety of objects can potentially enhance observation diversity and facilitate the agent’s learning of cross-modal alignment,

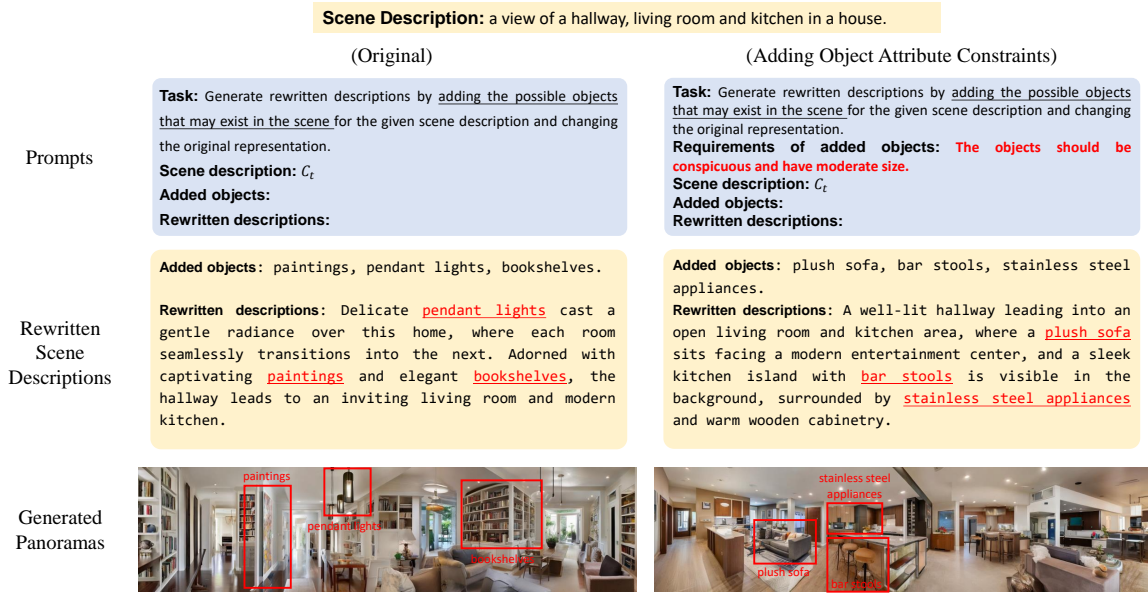


Fig. 9. Rewritten descriptions with different prompts and panoramas generated by T2I model with the corresponding rewritten descriptions. On the right side, we utilize the prompt adding object attribute constraints to generate rewritten description. Added objects in rewritten scene descriptions and generated panoramas are denoted in red fonts/boxes.

TABLE XIII
 ABLATION RESULTS ON OBJECT ADDITION AND OBJECT DELETION. WE CONDUCT THIS EXPERIMENT USING CLIP ViT B/16 AS VISUAL FEATURES.

Settings	Val Unseen	
	SR \uparrow	SPL \uparrow
baseline	72.37	58.75
object deletion	72.46	61.17
RAM(ours)	73.65	63.13

thereby improving navigation performance.

D. Controlled object generation

To investigate the potential of our RAM in controlled object generation for creating specific VLN scenarios, we incorporate the object attribute constraints on the LLM prompt presented in Fig. 9. From Fig. 9, we can observe that by adding the constraints, the LLM can successfully generate objects with desired styles, e.g., the “bar stools” and “plush sofa” which have a moderate size. And the T2IMs also successfully generate the desired objects in the panoramas. These results reveal the potential of extending our method to generate VLN scenarios with specific styles.

Algorithm 1: Mixing-then-Focusing Training Mechanism

Input : original real-world dataset $\mathcal{D}_{train} = \{\{O_t\}_{t=1}^T, I\}$, our rewritten dataset $\mathcal{D}'_{train} = \{\{O_t^r\}_{t=1}^T, I^r\}$,
navigation agent E^n

Output: trained agent E_{s2}^n

1: *for iteration in Stage 1 do*:

2: Use random observation cropping scheme (denoted as $\text{RC}(\cdot)$) to augment $\{O_t^r\}_{t=1}^T$, i.e., $\{O_t^r\}_{t=1}^T = \text{RC}(\{O_t\}_{t=1}^T)$;

3: Train E^n with $\mathcal{D}_{train} = \{\{O_t\}_{t=1}^T, I\}$ and $\mathcal{D}'_{train} = \{\{O_t^r\}_{t=1}^T, I^r\}$;

4: Optimize E^n based on loss \mathcal{L}_{s1} and get trained agent E_{s1}^n .

5: *end*

6: *for iteration in Stage 2 do*:

7: Train E_{s1}^n with $\mathcal{D}_{train} = \{\{O_t\}_{t=1}^T, I\}$;

8: Optimize E_{s1}^n based on loss \mathcal{L}_{s2} and get trained agent E_{s2}^n .

9: *end*

Algorithm 2: Data Augmentation Pipeline

Input : original panoramic observation O_t , original instruction I , scene description rewriting prompt P^c , instruction rewriting prompt P^i

Output: rewritten observations O_t^r , rewritten instruction I^r .

1: *for iteration in Object-Enriched Observation Rewriting do*:

2: **(1) Object-Enriched Scene Description Rewriting:**

3: Use the Vision-Language Model (VLM) to collect panoramic observation descriptions, i.e., $C_t = \text{VLM}(O_t)$

4: Obtain the rewritten object-enriched scene descriptions C_t^r accompanied by added objects $\{B_{t,n}\}_{n=1}^N$ with P^c and C_t , i.e., $C_t^r, \{B_{t,n}\}_{n=1}^N = \text{LLM}(C_t, P^c)$

5: **(2) Panorama-to-View Observation Generation:**

6: Obtain rewritten observations O_t^r by feeding C_t^r into the panoramic T2IM model, i.e., $O_t^r = \text{T2IM}(C_t^r)$

7: Use Equirec2Perspec algorithm to get single-view images, i.e., $\{O_{t,k}^r\}_{k=1}^K = \text{Equirec2Perspec}(J_{inv}, R, O_t^r)$

8: *end*

9: *for iteration in Observation-Contrast Instruction Rewriting do*:

10: **(1) Sequential Landmark Grounding:**

11: Use an LLM to extract the sequential landmarks $U = \{U_k\}_{k=1}^M$ from the original instruction I

12: Extract the ground-truth action (observation) G_t at timestep t from the original observation O_t

13: Employ CLIP [46] to find the matched landmark U_t for each G_t by taking the landmark U_k which has maximum similarity with G_t

14: **(2) New Observation Description Collection:**

15: Extract the ground-truth action (observation) G_t' which has the same position as G_t from the rewritten observations O_t^r

16: Adopt the VLM to generate the description C_t' for the ground-truth action (observation) G_t' , i.e., $C_t' = \text{VLM}(G_t')$

17: **(3) Instruction Rewriting by Observation Contrast:**

18: Acquire the rewritten instruction I^r by querying the LLM, i.e., $I^r = \text{LLM}(\{U_t\}_{t=1}^T, \{C_t'\}_{t=1}^T, I, P^i)$

19: *end*